Deformable Mirror Demonstration

Kristin Berry

Ashley K. Carlton

Zachary J. Casas

James R. Clark

Vladimir Eremin

Zaira G. Garate

Julian Lemus

Immanuel David Madukauwa-David

Tam Nguyen T. Nguyen

Paul Salcido

Alexandra E. Wassenberg

May 6, 2013

Contents

List of Figures

List of Tables

List of Acronyms

DeMi Deformable Mirror Demonstration

DM Deformable Mirror

FOV Field of View

PSF Point Spread Function

1 Introduction

1.1 Mission Statement

1.2 Motivation

2 Mission Overview

2.1 Requirements

2.2 Concept of Operations

2.3 N^2 Diagram

2.4 System Level Budgets

3 Subsystems

3.1 Payload

3.1.1 Requirements - AC

There are two types of payload requirements, the first set applies to the deformable mirror system. The second set pertains to the measurement and reconstruction of the wavefront. (All requirements are displayed in Appendix A.)

The deformable mirrors must operate for at least 5 minutes per orbit (PLD-1). This requirement comes from the mission level requirements (MLR-3, MLR-4) to characterize the deformable mirrors. The individual actuators that make up the deformable mirror must have a response time of less than or equal to 0.001 s, with a control rate of at least 100 Hz. The stroke must be at least 1.5 μm, with control precision of less than or equal to 1 nm.

The requirements on measuring and reconstructing the wavefront are requirements on the detector. Nominally, the detector must operate (take images) for at least 5 minutes per orbit, and be able to function at at least 10 Hz (PLD-2). The requirement is further separated into a Diagnostic Mode, used for calibration and for full frame images, and a Burst Mode, used for data capture. Diagnostic Mode is required to take images for at least a minute per orbit at 10 Hz (PLD-2.1). Burst Mode is required to take images for at least 30 seconds per orbit at least 100 Hz (PLD-2.2). For both modes, the reconstruction accuracy must be less

than or equal to 100 nm rms (PLD-2.3).

3.1.2 Trade Studies and Decisions Made - AC and KB

Payload Architecture - AC While in future applications the deformable mirror will be used to aid in observing stars or other objects, the mission goal is to characterize the deformable mirrors in an easy platform, making the internal laser source desirable for this technology demonstration. There are many different techniques to measuring and reconstructing a wavefront [17]. Only sensored approaches are considered for this platform due to the compact form factor and desire for simple components. There are many wavefront sensing approaches that could be implemented, as well as improved or modified versions of those presented here, which could be considered in future analyses, but the two approaches discussed in detail are a Michelson Interferometer and a Shack-Hartmann Wavefront Sensor.

Michelson Interferometer with Linear Stager The interferometer design shown in Figure 1 is slightly modified from a typical interferometer due to volume constraints on the payload and the requirement for high contrast imaging. It has an internal source (laser diode), whose path is denoted by a dotted red line. The laser beam is first resized, then is reflected 90 degrees by a flat mirror. The light is then divided by a beam splitter oriented 45 degrees to the beam. The transmitted beam travels to the deformable mirror where it is reflected back towards the beam splitter. Half of the beam is deflected by 90 degrees at the beam splitter and strikes the detector. The reflected beam travels to the flat mirror on the linear stager where it is reflected and half of it then is transmitted through the beam splitter and reaches the detector. The two beams that reach the detector interfere to produce fringes that are analytically well understood as a function of beam coherence/divergence and mirror tip/tilt [8] and that can be simulated for a variety of different deformable mirror shapes.

For this particular design, as mentioned previously, a flat mirror is on a piezo linear stager which moves in increments of fractions of the incoming wavelength. This allows for higher precision fringe patterns (reference?), allowing for better mirror characterization.

What is not shown in Figure 1 is the controller for the linear stager. It does not currently fit within the constraints of the satellite in terms of mass, volume, and power needs. It would require significant modifications, if it were to be implemented. Also, the additional moving part increases the risk and complexity of the mission.
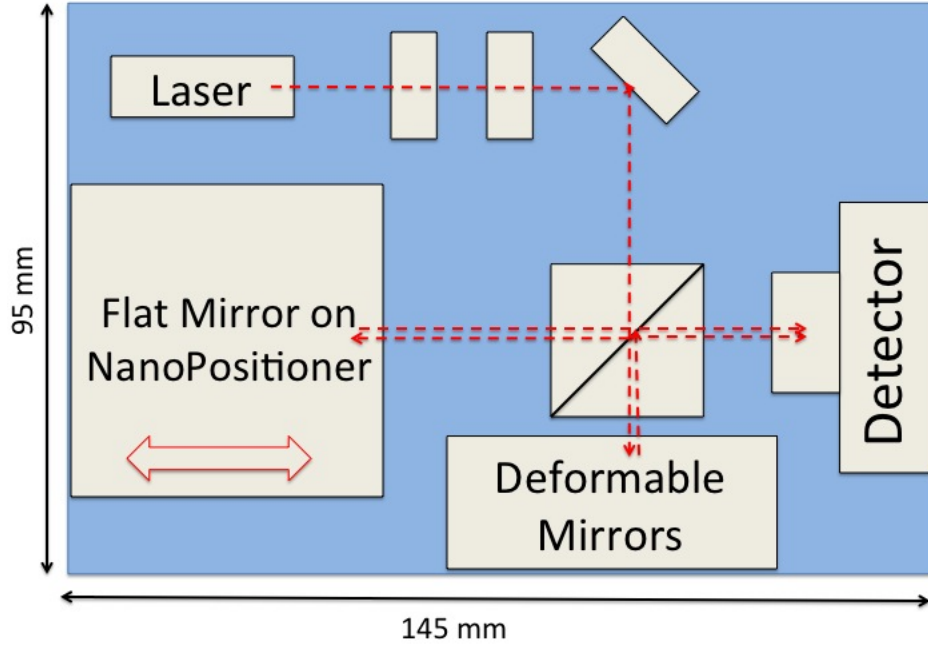
Figure 1: This is the Michelson Interferometer with the flat mirror on a linear stager. This is a payload design possibility.

Shack-Hartmann Wavefront Sensing System   For the wavefront sensing design in Figure 2, a Shack-Hartmann lenslet array on the detector is used, allowing for accurate wavefront measurement and reconstruction sensitivity. The design has an internal source (laser diode), whose path is denoted by a dotted red line, and an aperture for imaging an external source, whose path is denoted by a dotted green line.

For the internal source, the laser diode module emits a collimated elliptical beam. This beam enters a linear polarizer (where its intensity is halved). The beam then encounters a flat mirror at 45 degrees, reflecting the beam 90 degrees, and proceeds to a primary beam splitter. Here, the beam is reflected 90 degrees to secondary polarizing beamsplitter, and reflected another 90 degrees. The beam then goes through a quarter waveplate (where the beam is now elliptically polarized) before striking the deformable mirrors. The deformable mirrors reflect the beam back through the quarter waveplate, rendering the beam now linearly polarized with an orientation that allows it to pass through the secondary beam splitter. The beam then proceeds through the microlenslet array, creating a spot diagram on the detector corresponding to shape of the wavefront.

For the external source, the wavefront beam enters a plano-convex lens and then passes
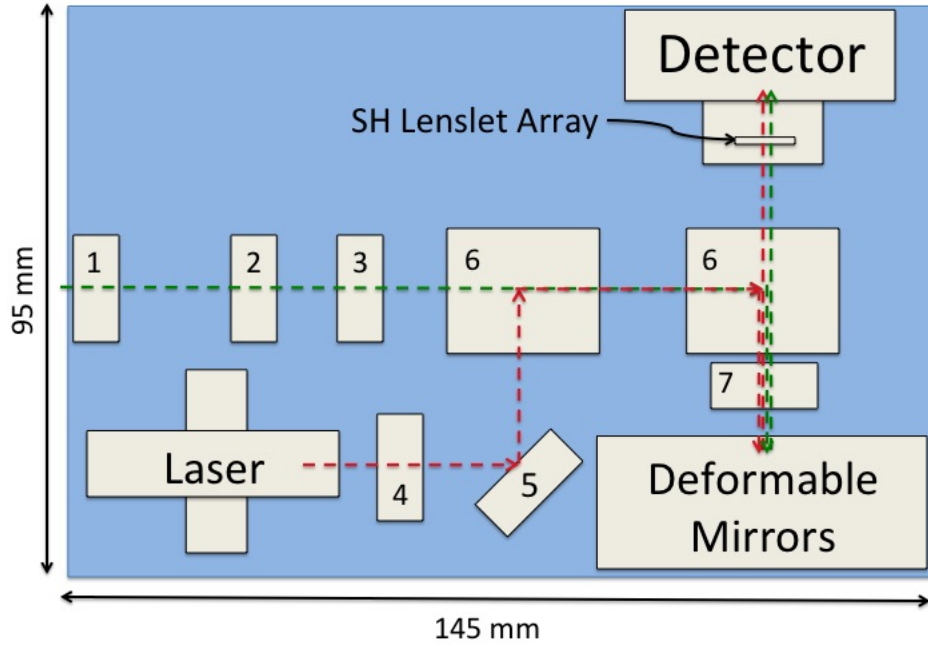
Figure 2: This is the Wavefront Sensing design with a Shack-Hartmann lenslet array. This is a payload design possibility.

through a collimating lens. The beam then enters a linear polarizer (where the intensity is halved). The beam then passes through the primary beam splitter, and then to the secondary polarizing beamsplitter, which reflects the beam 90 degrees towards the quarter waveplate and the deformable mirrors, as mentioned previously, and follows an identical path to the detector.

Design Decision The mission goal is to characterize the deformable mirror system, and to accomplish this with COTS as much as possible to allow for a quick and easy platform for space (MLR-3, MLR-4). While the interferometer with the linear stager is able to achieve higher precision, the Shack-Hartmann wavefront sensing system will fit with minor modifications to components, and allows for sufficient mirror characterization, meeting our mission goal and requirements. Therefore, the Shack-Hartmann wavefront sensing design in Figure 2 has been chosen to image the wavefront.

The chosen design allows the detector to image both an internal and external source. While the mission goal can be accomplished with just an internal source, the ultimate goal of using this technology on a larger space telescope for imaging of bright stars motivates the

use of an external source. Therefore, the option for an external source will be included in the design.

Due to the added complexity required of the ADCS system on a CubeSat platform, the external source imaging will not require knowledge of particular stars and navigating there. In contrast, with pointing knowledge from ADCS, the shutter on the aperture will be commanded open when a bright star is in the field of view (FOV). Additional work is need to evaluate revisit times to particular stars. Pointing requirements on the maximum ADCS slew rate to keep the star on the same pixels on the detector are discussed in Section **??**.

The aperture for imaging an external source will necessarily be small, given the volume constraints of the CubeSat platform after accommodating all of the key elements of the system (deformable mirror, mirror driver electronics, detector, and necessary imaging optics). Due to these key elements, it is not practical to design the external source imaging as a reflecting telescope. While it may be possible to accommodate a larger aperture lens ($> 60\,mm$), the corresponding longer focal length would not fit in the space, and the space for resizing the beam is limited. While the smaller aperture will limit the angular resolution and sensitivity and increase the size of the point spread function (PSF), tight angular resolution is not a requirement for this technology demonstration. Therefore, an aperture lens with diameter $12.7\,mm$ has been chosen, with a minimum focal length on the order of its diameter. Using the Rayleigh criterion, the angular resolution (width of the center of the PSF) at $500\,nm$ would be 2.436" (NEED TO CHECK number, because Im getting double this.).

The current design is an open loop system, where images and centroid solutions (reference to how centroids are found?) are sent to the ground, and analyzed there. Then, commands can be sent to the payload about how to correct the wavefront. However, the choice of a Shack-Hartmann design makes it easier to incorporate closed loop control for future follow up missions. The option of active correction of the wavefront on-orbit with the current design can be accomplished by the addition of a few components and requiring more on-orbit processing.

All optical elements of the system have been preliminarily chosen. See Appendix **??** for the full list of elements with part numbers and mass totals. Glass elements were chosen to be UV fused silica over other glasses whenever possible for their better performance in space [13] due to a high coefficient of thermal expansion and better UV transmission. All elements also have anti-reflective coatings that are efficient in the visible spectrum (400 - 700 nm). Mounts have been chosen for all components, however, these are only estimates of the custom mounts that will be built for all optics. The reason for this is due to the space

10

application. All elements must be mounted in stress-free mounts (no glass touching metal, etc.) and mounted to an optical breadboard with multi-footed lens tubes that are made of aluminum, or of a metal that has the same coefficient of thermal expansion as the lenses they hold. Future modeling and optimization of the optical design will yield more exact component choices.

Payload Operations For the initial demonstration and on-orbit testing, we will use an internal light source. This eliminates any payload specific requirements on the satellite's attitude and inclination. For the latter half of the mission, we will use an external light source, attempting to image the optical wavefront from a star.

After detumbling, and thirty days of commissioning, as describe in Section ???, the payload will perform a status check of all instruments. This includes the deformable mirror system, the detector, and the laser. Each element will be turned on and checked for any error or status codes. Then, the payload with take some TBD sequence of test images, with TBD sequence of mirror positions (not very many, not very frequently). The full-frame images will be sent down with centroid solutions and any available status information directly from the deformable mirrors and the detector.

The next phase is to calibrate the system. This involves turning on the laser and recording several images in this configuration with the detector, without deforming the mirrors (acts as a flat mirror). From these images, one can find the centroids and average them to obtain new 'standard centroids' which will be used for wavefront comparison calculations throughout the remainder of the mission. These images, averages, and new centroid solutions will be sent to the ground.

The next, and primary, stage is data capture using the internal source. The laser is turned on, then the mirror is deformed by a predetermined test sequence of commands, and the wavefront is imaged on the detector. The test sequence will include 'poking' one actuator at a time, and 'poking' combinations of actuators. Then, the images are read from the detector, centroids are found, and one full image and the collection of centroid solutions are sent down to the ground.

The second part of data capture will be with an external source. With knowledge from ADCS, the shutter will be commanded open, and the laser will be commanded off, allowing some TBD external source to be imaged. The images are read from the detector, the centroids are found, and one full frame image along with the collection of centroid solutions are sent to the ground. All downlinked files are timestamped.

Deformable Mirror System - KB

Detector - KB

Shack-Hartmann Lenslet Array - AC A Shack-Hartmann lenslet array consists of an array of lenses (called lenslets) of the same focal length, where the array is focused on the detector. Each lens creates a spot, creating a spot diagram on the detector. Figure 3 demonstrates incoming light through a lenslet array. The local tilt of the wavefront across each lens can then be calculated from the position of the focal spot on the sensor; the displacement, Δx, equals the local slope of the wavefront. Any phase aberration can be approximated to a set of discrete tilts. By sampling an array of lenslets all of these tilts can be measured and the whole wavefront approximated. One thing to note: since only tilts are measured, the lenslet array cannot detect discontinuous steps in the wavefront.
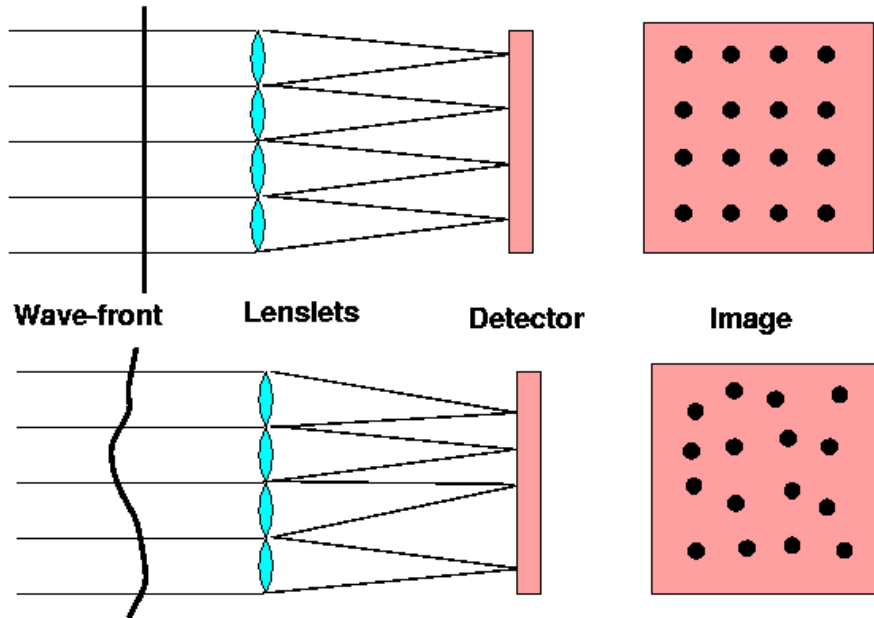
Figure 3: This figure demonstrates the result of two wavefronts, plane and abberated, entering a Shack-Hartmann lenslet array, and their resulting spot diagrams on the detector.

To get the best measurement of the wavefront, the maximum number of spots, and therefore lenses, is desired. As a result, for a constant beam size, a lenslet array should be chosen with the lowest pitch (distance from the center of each lens) in order to get the maximum number of spots for the beam.

12

Therefore, MLA150 (Figure 4) was chosen from ThorLabs, with a pitch of 150 μm. The lenslet is 10 mm^2 square, so it contains about 66 by 66 microlenses. It has a 9 mm^2 square effective aperture, with a focal length of 5.2 mm, and will be mounted in the lens tube on the detector (see Paragraph **??**). For an approximate beam size of 2.25 mm (see Paragraph **??**), approximately 15 by 15 lenses will be used of the lenslet array. As discussed in Paragraph **??**, a 2.25 mm incoming beam corresponds to about 425 px^2 square, allowing for over 20 pixels per spot, so there is no concern for multiple spots falling on the same pixel.
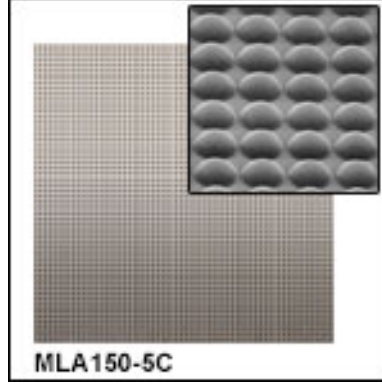
Figure 4: This is the MLA150 lenslet array from ThorLabs choosen for the Shack-Hartmann Wavefront Sensing design.

3.1.3 Analysis

3.1.4 Summary of Outputs - AC

The payload's operational requirements are major drivers for the design of the rest of the satellite. A summary of mass totals, power needs, and thermal requirements of all major Payload components can be found in Table 1. During data capture mode, the payload needs to be kept within 0°C to 50°C, will draw a maximum power of 4.5 W, will output a maximum data rate of 550 $Mbit/s$, and, during external data acquisition only, has a maximum slew rate of 4.7$'/s$. With all components, the Payload is about 997 g, or 1.25 kg with a 25% margin.

3.1.5 Risks

¡¡¡¡¡¡¡ HEAD

Table 1: This is a summary of the mass totals, power needs, and thermal needs of the major payload components.

Component	Mass (g)	Power (W)	Thermal, operating (°C)	Thermal, storage (°C)
Laser diode	24.45	0.0045	−10 to 50	unknown
Detector	46.64	$< 2\ W$	0 to 50	−20 to 80
Def. Mirrors + Driver	189.9	$< 2.5\ W$	−10 to 50	unknown
Optical Breadboard	∼ 250			
Optical Enclosure	∼ 300			
Totals	996.9	$4.5\ W$ max	0 to 50	−20 to 80

3.1.6 Future Work

3.2 Power - JC

3.2.1 Requirements

The Power subsystem is required to supply power to all other subsystems under all conditions. In particular, it must supply an average of 3.54 watts on average over the course of the orbit (calculated in Section 3.2.4, Analysis), sustain a maximum load of 13.84 watts during certain operational modes (downlink mode, per Systems), have a minimum battery capacity of 3.9 watt-hours (calculated in Section 3.2.4, Analysis), and meet these requirements for up to 1 year, or approximately 6,000 cycles (calculated in Section 3.2.4, Analysis).

3.2.2 Trade Studies and Decisions Made

Using STK, we compared the average power obtained by the solar panels under several circumstances. The two variables were the inclusion or omission of a solar panel on the top face of the satellite, in addition to the four side-mounted panels, and the orientation of the satellite in its orbit – whether it few "face-first", with the normal vector of one of its sides aligned with its velocity, "corner-first", where it is tilted by 45 degrees about its long axis from the face-first orientation, or spinning about its long axis. The face-first and corner-first attitudes are illustrated below:

Note that these power values are averaged over the entire orbit – that is, taking the incoming power to be zero during local night and including that in the average. This was done because the satellite is active during the entire orbit, and its average power needs are calculated over the entire orbit; to ensure that we are comparing likes against likes, we did the same for the power generated.
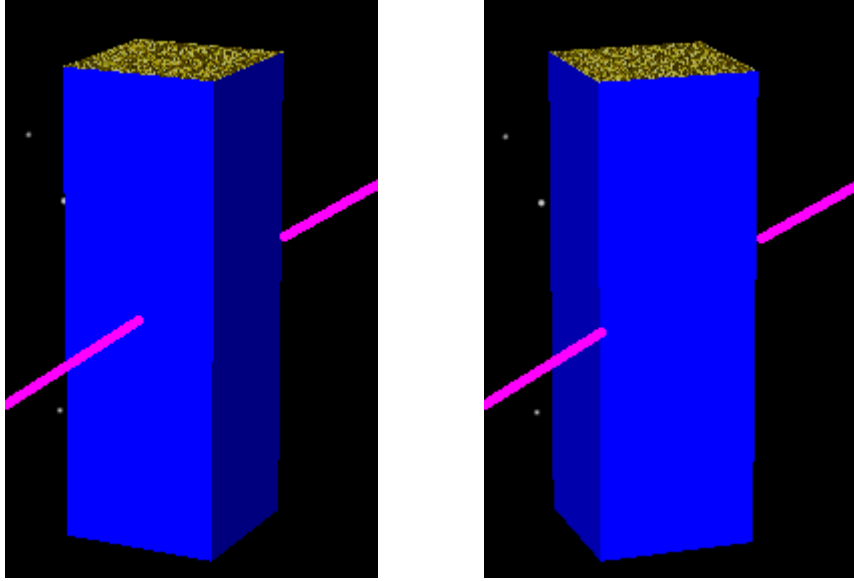
Figure 5: The "face-first" and "corner-first" attitudes. Images generated from STK.

Table 2: Power values for various panel configurations and satellite attitudes.

	Face-first	Spinning	Corner-first
Side panels	3.77 W	4.16 W	4.52 W
Side and top panels	4.45 W	4.84 W	5.19 W

3.2.3   Decisions Made

In general, the power subsystem was designed to be as simple as possible while meeting the satellite's power needs. We chose to use stock parts as much as possible because they have known performance, which helps us verify that requirements are met and reduces the margins we need to hold.

The chosen solar panel configuration was four body-mounted side panels. Body-mounted panels were chosen over deployable panels because they minimized the surface area of the satellite, which minimized the disturbance torques, and they are symmetrical, reducing the pointing constraints on the ADCS. The satellite would be oriented in a nadir-pointing configuration, so the nadir face would almost never see any sunlight, so we chose not to panel it, and we chose not to panel the zenith face to allow the payload to have an aperture in that face, so that it could potentially image external light sources.

The remainder of the power system is similar to that of most other satellites: an elec-
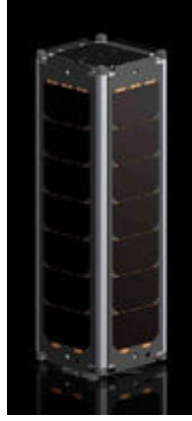
Figure 6: The solar panel configuration to be used on the DeMi satellite. Image from Clyde Space.[1]

trical power system module takes power from the solar panels and manages the current and voltage levels to ensure that the panels deliver power at maximum efficiency, a secondary (rechargeable) battery supplies the satellite with energy during eclipse, and a power distribution module supplies power to systems which are not part of the main system stack, like the torque coils.

The satellite's power subsystem does not include a primary battery. A primary battery was never included in the design because the satellite was to be covered on most sides by solar panels and would be power-positive in detumbling mode, so it would charge as soon as it exited the P-POD. The only reference to a Cubesat containing a primary battery was a description of a Cubesat that lacked solar panels entirely.[2]

3.2.4   Analysis

The average power required is the time-weighted average of the power required during the various modes of the satellite:

$$P_{req,avg} = \frac{1}{T_{total}} \sum_{modes} \sum_{systems} T_{mode} \, P_{sys,mode} = 3.54 \text{ W} \tag{1}$$

The solar panels are required to gather enough power during the day to power the satellite for the entire orbit, when taking the inefficiency of the EPS into account ($\eta = 0.85$ in the worst case[3]):

$$P_{req,panels} = \frac{T_d + T_e}{T_d} \frac{P_{req,avg}}{\eta} = 6.61 \text{ W (cold)}, 5.21 \text{ W (hot)}, 4.16 \text{ W (orbit avg)} \qquad (2)$$

"Hot" and "cold"[1] here refer to the two orbital cases which have the most and least solar exposure for the satellite because the orbit is fixed in inertial space, it appears to rotate with respect to the Earth-Sun vector over the course of a year. Every six months, it goes from a cold orbit, which is in the sunlight 63% of the time, to a hot orbit, which is 80% sunlit, and back again. The two orbits are illustrated below.
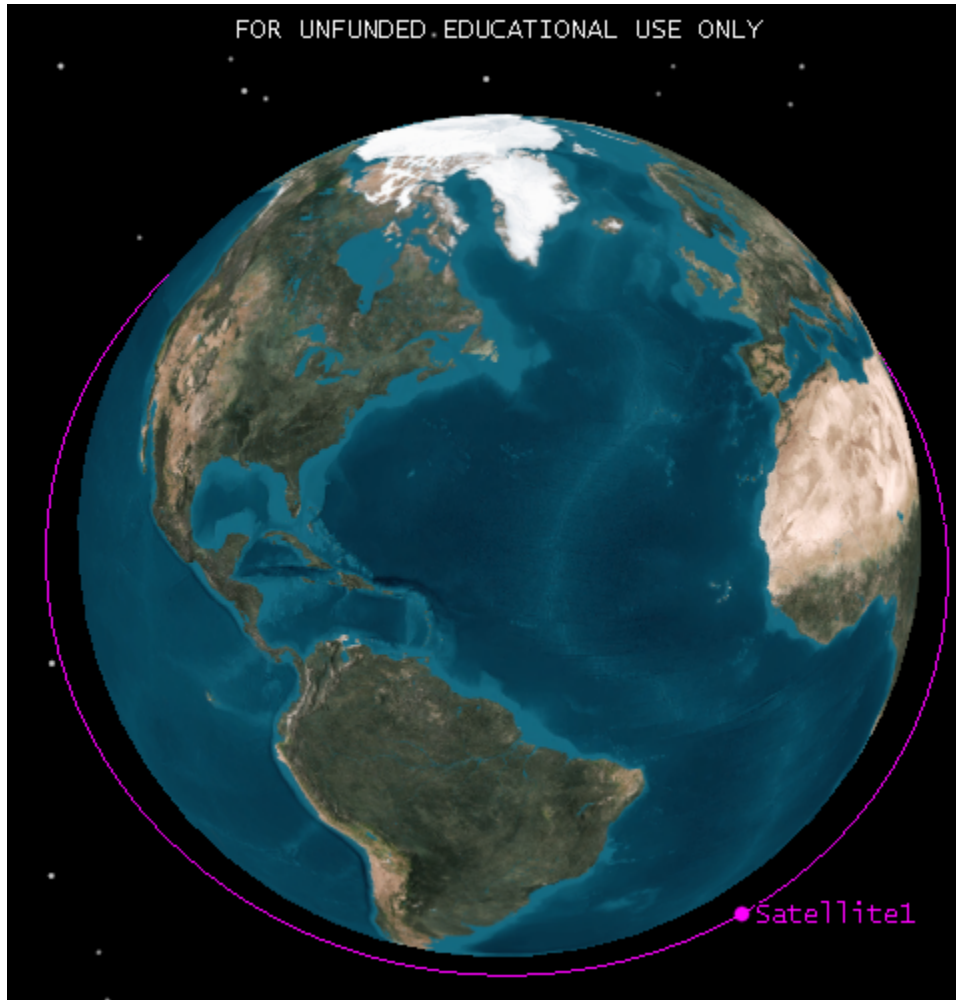
Figure 7: A "hot" orbit, where the satellite is exposed to the sun 80% of the time. Image generated from STK.

---

[1]Perhaps "bright" and "dark" would be better terms from a power perspective, because it is not temperature that gives us power but sunlight.
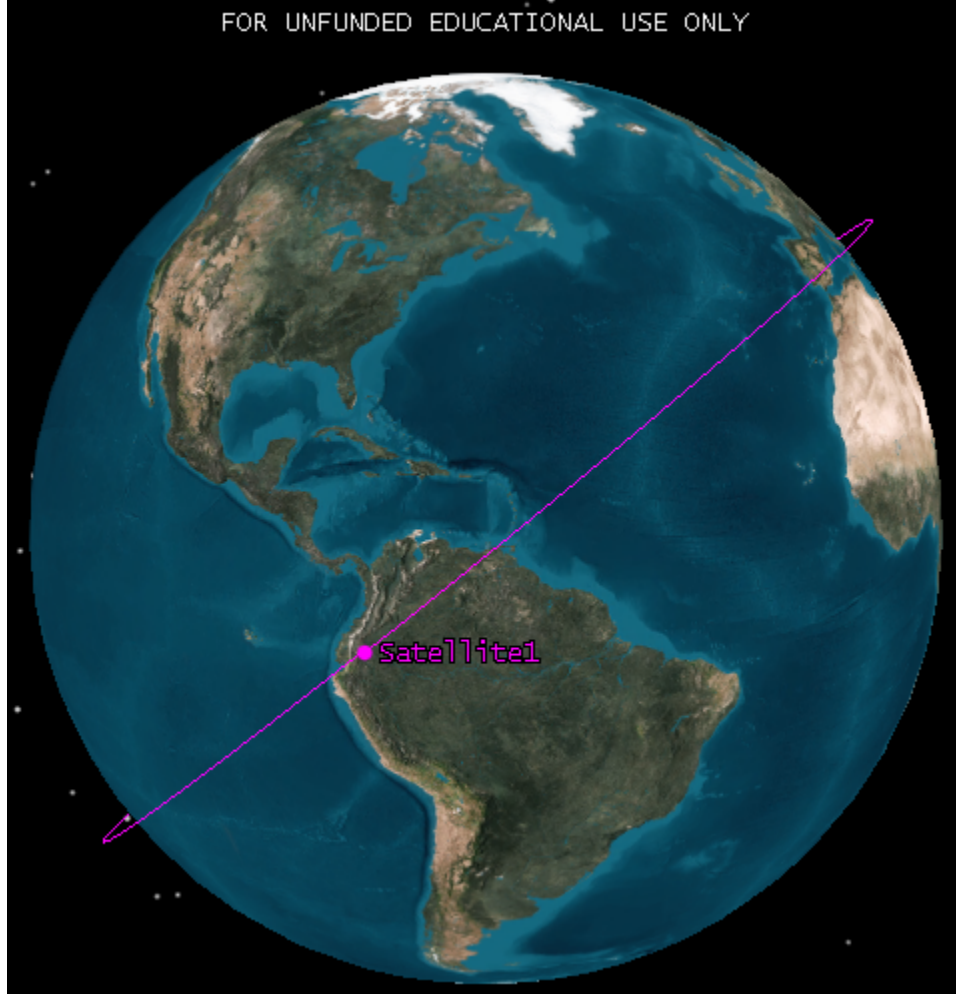
Satellite1

Figure 8: A "cold" orbit, where the satellite is exposed to the sun 63% of the time. Image generated from STK.

The satellite drains the most energy from the battery if it performs a ground station pass (maximum duration: 9.77 minutes, per Comm) and scientific operation (nominal duration: 5 minutes, per Payload) during local night:

$$E_{req,batt} = T_{sci}P_{sci} + T_{comm}P_{comm} + (T_e - T_{sci} - T_{comm})P_{standby} = 3.9 \text{ Wh} \tag{3}$$

The excess power is the power actually generated by the panels that does not go into powering the satellite or charging the battery – in other words, the difference between the power required power and the power actually generated:

$$P_{excess} = P_{panels} - P_{req,panels} = 0.63 \text{ W (cold)}, 2.57 \text{ W (hot)} \tag{4}$$

It can be useful to model the excess power as an average over the entire orbit, rather than just happening during local day (for first-order approximations of the equilibrium satellite temperature):

$$P_{excess,avg} = P_{excess} \frac{T_d}{T_d + T_e} = 0.40 \text{ W (cold)}, 2.06 \text{ W (hot)} \tag{5}$$

The number of charge-discharge cycles of the battery is approximately equal to the number of orbits that the satellite will have to sustain:

$$N_{cycles} = \frac{T_{year}}{T_{orbit}} = 5500 \approx 6000 \text{ (with 10\% margin)} \tag{6}$$

3.2.5 Summary of Outputs

Table 3: Outputs to other systems (mass, volume, power consumed, and survival and operating temperatures).[3] [4] [5] [6]

Component	Mass (kg)	Volume (U)	Power consumed (W)	Survival temperature (° C)	Operating temperature (° C)
Solar panels	0.540	0	0	-40 to 80	-40 to 80
EPS	0.083	0.15	0.1	-50 to 100	-40 to 85
Battery	0.256	0.2	0.1	-10 to 50	0 to 50
PDM	0.060	0.25	0.16	-50 to 100	-40 to 85
Total	0.939	0.6	0.36	N/A	N/A

The solar panels do not literally have zero volume, but because they are fixed to the sides of the Cubesat, they do not occupy any of the three units of internal volume.

3.2.6 Risks

The primary risk facing the Power subsystem is that our incoming power is fundamentally limited, so we will have to be careful to not exceed our budget. As computed in Analysis (Section 3.2.4), the average power drawn by the satellite for nominal mode durations is 3.54 watts. While the orbit-averaged power coming in from the solar panels is 4.52 watts, which is a 28% margin over the power needs, when we take the worst-case efficiency of the EPS's solar-panel connection into account[3], we find that as little as 3.84 watts are actually getting to the battery power bus, leaving only a 9% margin (which might then be further eroded

by inefficiencies in the power lines). This is less than the 18% margin goal we had set for ourselves, and substantially less than the 30% margin that JPL informed us was their usual standard for satellite missions.

This risk is mitigated by the 32% margin of available power over the standby power need of 2.91 watts. From this, we can be confident that, even in the worst possible case, the satellite will be power-positive during its standby mode. This means that, if the satellite should find itself unable to meet its power needs for nominal mode durations, it could be commanded to spend more time in standby mode and less in data capture or downlink mode to restore balance to its power budget. As mentioned in the Analysis section, the available power was calculated for the coldest, darkest orbit that the satellite will be in. For the brightest orbit, the average power generated by the solar panels over the entire orbit increases to 7.42 watts, which, taking the worst-case EPS efficiency into account, results in 6.31 watts reaching the power line, which is a 78% margin over the average power required. In fact, we could spend 29 minutes – nearly six times the nominal data capture mode duration – of such a bright orbit in data capture mode (leaving the downlink mode duration constant, as ground pass durations are independent of available power) while maintaining a 30% margin of available (post-EPS) power over required power. We can thus be assured that, even if the satellite is forced to reduce the duration of data capture and downlink modes during darker orbits to conserve power, we can make up for any shortfalls of captured data during better orbits.

3.2.7 Future Work

The performance of the solar panels and batteries is temperature-dependent. In particular, the battery becomes more effective as its temperature increases, while the solar panels become less so. Going forward, it would be useful to perform a more detailed simulation of the satellite that incorporates a thermal model, so that we can more accurately measure the effect of satellite temperature and dissipated excess energy (energy from the solar panels that does not go into charging the battery or powering the satellite).

=======

3.2.8 Future Work - AC

- Optical Modeling in ZEMAX: Determine final beam profile on the detector, Optimization of space to find the best choice of components, Explore thermal effects on beam and optical components

20

- Interferometer with Linear Stager Design Feasibility: Can nanopositioner elements be scaled down for a CubeSat platform?, What would the effects be on other subsystems?

- Imaging External Sources: Need to determine when and how to image an external source (FOV, star sensors)

- Closed Loop Control: Determine difficulty in implementation

- Stroke Analysis: Study properties of DM stroke

3.3 Power

¿¿¿¿¿¿¿ 7b454c39685a15bd7bc963104117aa5faf9dfebc

3.4 Communication

3.4.1 Requirements - ZC

Most of the Communications requirements (see Appendix A) are standard Communications requirements for operability. Comm-1 is simply stating what the main goal of the Communications subsystem is. Comm-2 is there to ensure that the link with the ground station is good enough to transmit all of the data that we need to. Comm-2.1 is there so that if there is an error in the transmission, the system will be able to realize this and ask for a correction. Comm-2.2 is so that it doesnt try to downlink more data than possible because if it does, then data will be lost. Comm-3 is simply there so that the Communications subsystem can ensure access with the ground station. Comm-3.1 and Comm-3.2 are specifics when it comes to communicating with the ground station. Comm-4 is there because if we do not encrypt it, another satellite may be able to receive our commands and learn about the DeMi system. Comm-5 is there to ensure that if there are errors, there will be very few of them. Comm-6 is just to ensure that DeMi follows all regulations set by different government agencies.

3.4.2 Trade Studies - ZC

The main factor in choosing what transceiver to use in our system is the data downlink amount. Because payload is generating so much data, Communications will need to have a high downlink rate to ensure that all of that data can be sent to the ground. Several options were looked into, and shown in Table 4.

Table 4: Communications Trade Study for Maximum Downlink Data Rate

Tranceiver	Maximum Downlink Rate
Espace Payload Telemetry System	1 Mb/s
AstroDev Li-1 UHF Transceiver	38.4 kb/s
ISIS TXS Small Satellite S-Band Transmitter	100 kb/s
Tyvak UHF Transceiver	200 kb/s
L-3 Cadet Nanosat UHF Radio	1.5 Mb/s
Microhard MHX2420 Modem	230.4 kb/s

3.4.3 Decisions Made - ZC

Given the information in Section 3.4.2, the L-3 Cadet Nanosat UHF Radio was chosen for use on DeMi. It will transmit at the frequencies and data rates outlined in the requirements, which are $445 - 455\ MHz$ for uplink at $19.2\ kb/s$, $460 - 470\ MHz$ for downlink at $1.5\ Mb/s$. The transceiver also has an extra $4\ GB$ of storage that avionics will be able to use in addition to any of its storage.
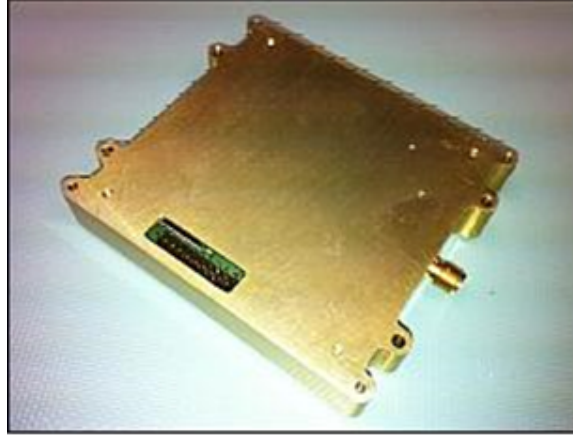
Figure 9: Photo of the custom-designed high-speed L3 Cadet radio [9].

Because the transceiver will be transmitting and receiving at UHF frequencies, a very common antenna choice is to use a measuring tape antenna that is tuned to the frequency that is desired. Because the antenna works like a quarter-wave monopole, one can determine the desired length of the antenna by dividing the wavelength of the transmitted and received signal by 4. Because the transmitting and receiving frequencies are different, the average of these frequencies was used to compute the wavelength.

$$\lambda = c/f \tag{7}$$

Eq. 7 is used to calculate the wavelength. λ is the wavelength, c is the speed of light, and f is the frequency. Using the average frequency of 465 MHz, the wavelength equals 0.645 m. Then to determine the length of the antenna one can just use the following equation.

$$l = \lambda/4 \tag{8}$$

In Eq. 8, l is the length of the antenna, and λ is the wavelength. Using a wavelength of 0.645 m, one can find that the desired length of the antenna is about 0.164 m. The gain of this antenna will be approximately 3 dB and the beam width approximately 65°.
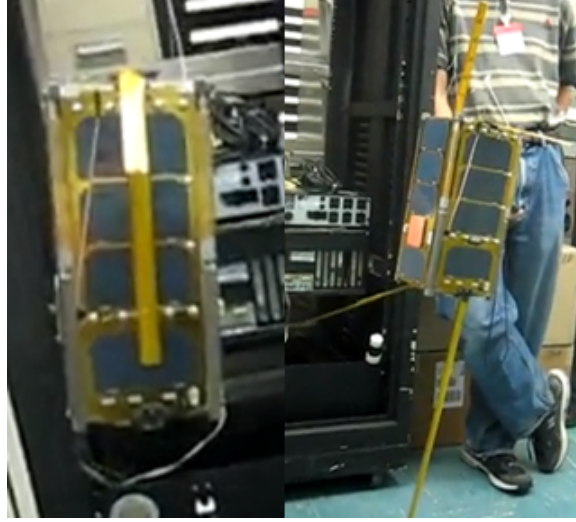
Figure 10: Photo of stored and deployed measuring tape antenna. The pictured CubeSat has four antennas. DeMi will only be using one [11].

The ground station that will be used with this system will be the NASA Wallops UHF Ground Station. This was chosen because the transceiver that will be used was also used in the Dynamic Ionosphere CubeSat Experiment, and the ground station that was used in that mission was the NASA Wallops UHF Ground Station. The diameter if the dish is 18.29 m, the gain is 35 dB and the beam width is 2.9°.

3.4.4   Analysis - ZC

One can calculate the maximum amount of data downlink per pass-by by multiplying the downlink data rate and the access duration per pass-by. Given the downlink data rate of

1.5 Mb/s, and the access duration of 586 s per pass-by, the maximum amount of data that can be downlinked in one pass-by is 109.9 MB. To account for the fact that the data-rate wont always be able to be at its maximum, and also for space for telemetry data and error correcting code, we have a margin of a factor of 2, so the maximum amount of data from payload that can be downlinked per pass-by is about 54.95 MB. Although this is not as much data as payload is creating, there will be on-board processing so that the amount of data that needs to be downlinked is below the maximum amount that is allotted for payload.

A Link Budget was created in order to determine the Link Margin for a worst case and a best case for uplink and downlink. Appendix B detail these budgets.

The first calculation in the Appendix B is to calculate the worst case propagation path length. We know that the best case length is 500 km because that is the altitude at which the satellite is orbiting. Figure 11 shows how a wave propagates through that atmosphere and will be explained beneath.
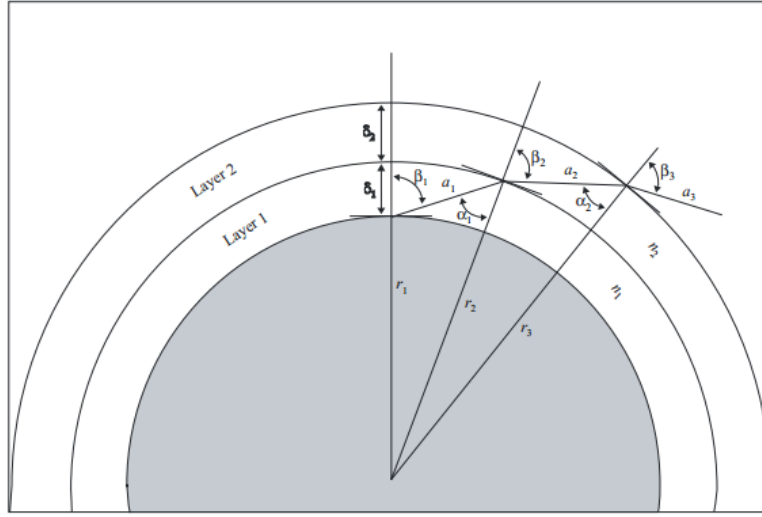
Figure 11: Diagram of propagation path of a signal from a satellite [12].

In order to determine the propagation path length, r, one must determine the path length of the first layer and the second layer and add them together. The equation for calculating [12] the path length of a layer is as follows.

$$a_n = -r_n \cos(\beta_n) + \frac{1}{2}\sqrt{4r_n^2 \cos^2(\beta_n) + 8r_n\delta_n + 4\delta_n^2} \tag{9}$$

In Eq. 9, a_n is the path length through layer n, r_n is the radii from the center of the Earth to the beginning of layer n, β_n is the exiting incidence angle, and δ_n is the thickness of layer n. The angle β_n can be calculated [12] using the following equation.

$$\beta_{n+1} = \arcsin\left(\frac{n_n}{n_{n+1}} \sin(a_n)\right) \tag{10}$$

In Eq. 10, n_n is the refractive index of layer n, and α_n is the entry incidence angle. Angle α_n can be calculated with the last equation needed in order to calculate [12] the propagation length.

$$a_n = \pi - \arccos\left(\frac{-a_n^2 - 2r_n\delta_n - \delta_n^2}{2a_n r_n + 2a_n\delta_n}\right) \tag{11}$$

Values that still need to be defined are β_1 (because it cannot be calculated using Eq. 11), δ_1, δ_2, n_1, and n_2. β_1 is just equal to the complimentary angle to the minimum angle at which the Wallops Ground Station can track, which is $5°$. δ_1 will be equal to the altitude at which the atmosphere ends which one can say is about $100\ km$. δ_2 is just the orbiting altitude minus δ_1. n_1, which is simple the refractive index of air, is 1.000293. The last remaining value to be defined is n_2, which is the refractive index of a vacuum, which is just 1. Using these equations, one can find that a_1 equals $707\ km$, and a_2 equals $1375\ km$. This means that the worst case propagation path length is equal to $2082\ km$.

The next value calculated in the Link Budgets is the Equivalent, Isotropic Radiated Power (EIRP). In order to calculate the EIRP [18], the following equation should be used.

$$EIRP = P_{tx} + G_{tx} - L_{output} \tag{12}$$

In Eq. 12, P_{tx} is the transmitter power, G_{tx} is the transmit antenna gain, and L_{output} is the output loss which is equal to all losses associated with the transmitter. All of these values can be found in the Link Budget (Appendix B).

Another calculated value in the Link Budget is the Space Loss. This is the loss of the signal as it is transmitted through space. It can be calculated [18] using the following equation.

$$L_s = 92.45 + 20\log_{10}(r) + 20\log_{10}(f) \tag{13}$$

In Eq. 13, L_s is space loss, r is the propagation path length, and f is the frequency of the transmitted signal. All of these values can also be found in the Link Budget (Appendix B.

The next equation can be used to calculate [14] the transmitting antenna temperature.

$$T_{antenna} = \eta T_{sky} + (1 + \eta)\frac{T_{sky} + T_{ground}}{2} \tag{14}$$

In Eq. 14, η is the antenna efficiency, T_{sky} is the temperature of the space behind the receiving antenna. The temperatures used for uplink are determined by using the background temperature of space. For downlink, the temperature of the Earth is used. T_{ground} is the temperature of the ground around the antenna. For uplink, this is the temperature of the Earth, and for Downlink, it is the background temperature of space.

The system noise temperature, T_{sys}, is calculated by adding the transmitting antenna temperature and the receiver temperature [14]. The receiver temperature for both cases is unique to the receiver and can be determined by the manufacturer.

The next calculated value is the Receiver Gain to Noise Temperature. This is computed [18] using the following equation.

$$\frac{G}{T} = G_{rx} - T_{sys} \tag{15}$$

In Eq. 15, $\frac{G}{T}$ is the Receiver Gain to Noise Temperature, G_{rx} is the receiving antenna gain, and T_{sys} is the system noise temperature. Using $\frac{G}{T}$, the total losses in the system, and EIRP one can determine [18] the Receiver Carrier to Noise Ratio.

$$\frac{C}{N_0} = EIRP + \frac{G}{T} - L_{total} + 228.6 \tag{16}$$

Using that value and the data rate in decibels, one can calculate [18] the Energy per bit to Noise Ratio.

$$\frac{E_b}{N_0} = \frac{C}{N_0} - R_b \tag{17}$$

Finally, the link margin can be determined by subtracting the required Energy per bit to Noise Ratio from the predicted one.

3.4.5   Summary of Outputs - ZC

There were several outputs during the design process from the Communications subsystem. These outputs include the Ground station to Orbits, which is NASA Wallops UHF Ground Station, the beam width of Wallops UHF Ground Station and DeMi to ADCS, which are 2.9° and 65° respectively, the operational and survival temperatures of the transceiver to Thermal, which are −20° C to 70° C and −40° C to 80° C respectively. The power for each mode to Power, and the mass and volume to Structures are detailed in Table 5
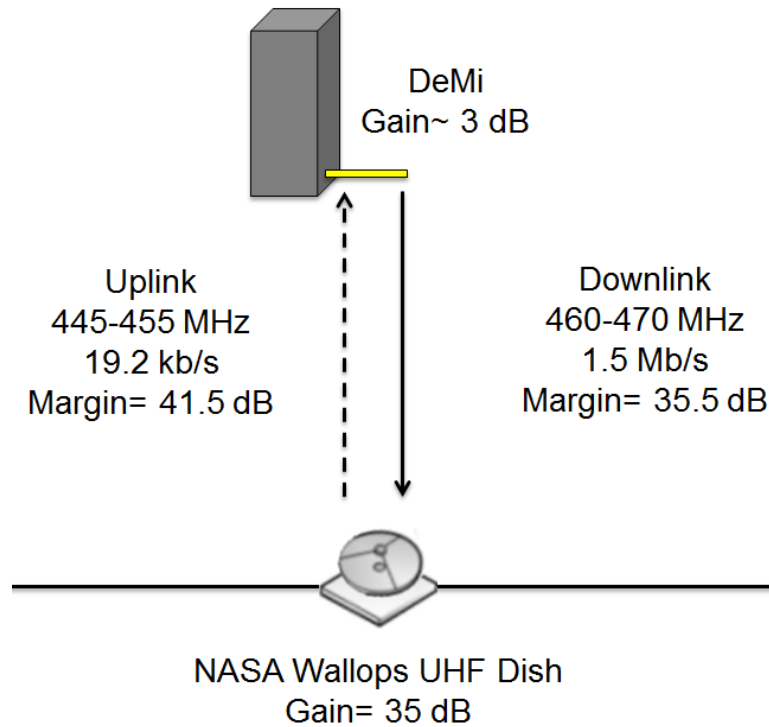
Figure 12: Representation of Satellite and Ground Station during Best Case Communication.

3.4.6 Risks - ZC

As of PDR, there were no risks for the Communications subsystem. Towards the beginning of the design process, there were huge concerns about Communications not being able to downlink enough of the data from Payload, but since then, Avionics has decided that DeMi will be doing on-board processing so that all of the data does not need to be downlinked.

3.4.7 Future Work - ZC

Moving on from here, the main thing that should be done is research and analysis of measuring tape antennas. There is currently not very much information out there that is available to DeMi concerning them, so research to determine the exact gain, beam width and radiation patterns should be conducted.
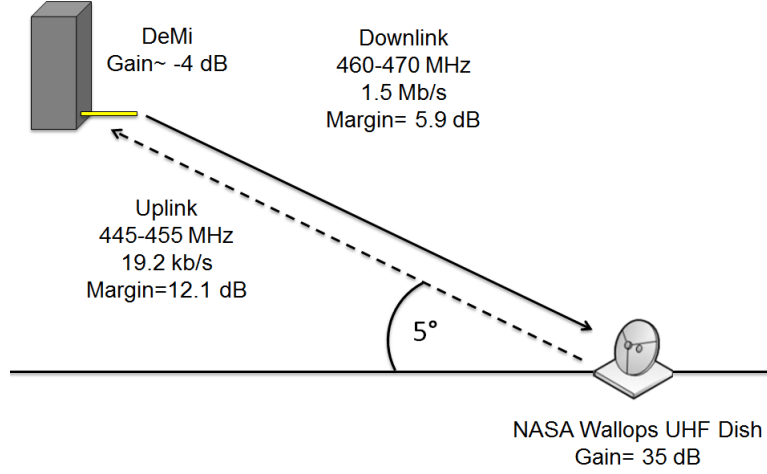
Figure 13: Representation of Satellite and Ground Station during Worst Case Communication.

Table 5: Communications Budgets

Output	Value
Power (Standby)	0.51 W
Power (Data Capture)	0.51 W
Power (Downlink)	11.44 W
Power (Uplink)	0.51 W
Power (Safe Mode)	0.51 W
Mass	0.235 kg
Volume	0.069 U

3.5   Avionics

3.5.1   Requirements - VE

The Avionics subsystem requirements are presented in Appendix A. The main driving requirements are number 3 and 2 in the order of importance because they are the most challenging to satisfy with a current level of technology.

3.5.2   Trade Studies - VE

We have two main options that are able to satisfy the requirements for Avionics subsystem. Both are shown in Table 6

Since we have identified the Payload driven requirements as the most challenging, we

Table 6: Hardware Options

	Processing on-board	Raw images to the ground
Component Name	The Steepest Ascent Mission Interface Computer CS-MIC-G-EM	Single Board Computer Motherboard + PPM with TI MSP430F2618
Power Consumption	0.5 − 1.25 W	10 mW
Capabilities	Telemetry/Telecommand + Real time image processing on FPGA	Telemetry/Telecommand
Storage Capacity	Up to 16 GB	Up to 2 GB
Processors	TI MSP430 + Xilinx FPGA (model can be selected)	TI MSP430F2618
Interfaces	I2C, SPI, UART	I2C, SPI, UART
Mass	62 g	88 − 114 g

have to start selection of appropriate hardware from that.

Table 7: Payload image capturing modes

Mode	640x480 px subframe	640x480 px subframe	1280x1024 px full frame
Frame Rate	100 fps	10 fps	10 fps
Data Rate	310 $Mbit/s$	31 $Mbit/s$	131 $Mbit/s$
Duration	30 s	300 s	60 s
Memory Required	1.14 GB	1.14 GB	0.96 GB

Lets consider approach when we downlink all the data generated by the Payload without processing it. From Table 7 we can see that Payload will be generating around 1 GB of data every time it is run. For a given 1.5 $Mbit/s$ downlink speed in this case we will need 600 s to downlink all the data captured or 10 ground accesses. Since we have only one ground access every three orbits in general this particular approach seems to be too ineffective in terms of Payload active time.

Thats why we mainly consider the second approach when we do all necessary calculations onboard and send only results to the ground. It dramatically reduces the amount of transferred data to around 10 − 100 KB instead of gigabytes and enables to implement a closed loop deformable mirror control system.

After we have solved a problem with data storage we can focus on the core of every

Avionics subsystem - its processor. Now we have higher but still reasonable requirements for processing power according to the computation tasks that it will be solving: 1. Centroid, delta x and delta y, slope reconstruction, and 2. Linear algebra for mirror controller. The Steepest Ascent Mission Interface Computer CS-MIC-G-EM is a good fit for such tasks because it has an FPGA to be configured for image processing and a microcontroller for general tasks such as telemetry and ADCS computations.

3.5.3   Decisions Made - VE

We have made a decision to use CS-MIC-G-EM (Figure 14) mainly because it enables on-board image processing which reduces the amount of data we send to the ground and provides with a capability to build a closed loop deformable mirror control system.

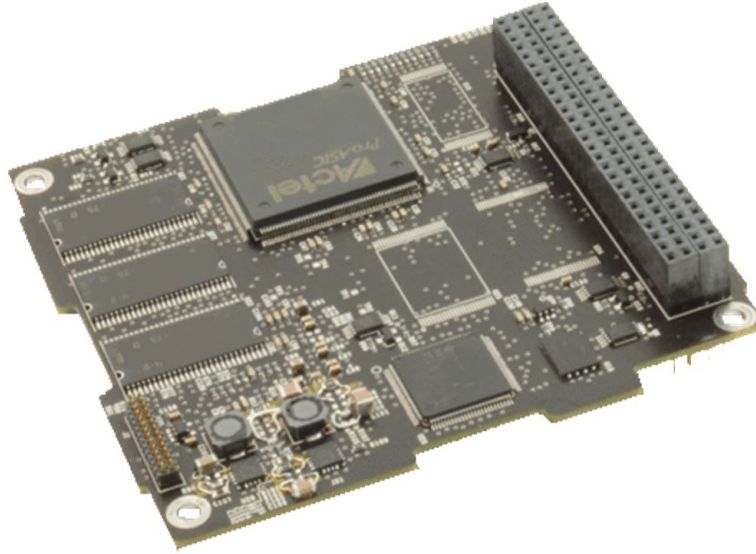Figure 14: Mission Interface Computer CS-MIC-G-EM [15]

It is also capable of providing the following interfaces with other subsystems see Table 8.

3.5.4   Analysis - VE

The system architecture in general is shown in Figure 15. The Mission Interface Computer we have selected allows us to separate telemetry from image processing data. The first is processed on CPU while the latter is done on FPGA.

Table 8: Avionics hardware interfaces with other subsystems (*assuming update 10 times per second).

Subsytem	Component	Interface	Data rate
Payload	Detector (IDS UI-5241LE-M)	GbE	550 $Mbit/s$ max
	Mirror driver (BMC Mini-Driver)	USB 2.0	480 $Mbit/s$ max
	Laser (ThorLabs CPS 186)	GPIO	–
Power	EPS, PDM	12C	400 $Kbit/s$ max
ADCS	5 sun sensors	analog	100 bit/s*
	ADIS16305 IMU/Magnetometer	SPI	160 bit/s*
	Torque coils	12C (via PDM)	–
Thermal	14 Temperature Sensors	analog	100 bit/s*
	Thermal Heater	12C (via PDM)	–
Communication	Cadet NanoSat UHF Radio	RS232	1.5 $Mbit/s$

3.5.5 Summary of Outputs - ZC

The Avionics system had very few outputs to the other subsystems. It had to give values to Thermal for operational temperature range for the computer which is $-25°$C to $85°$C. The survival temperature is unknown. It also had to give outputs to power for power consumed during the different modes, and to structures for the mass and volume. These outputs, or budgets are detailed in Table 9.

Table 9: This is a summary of the mass totals, power needs, and thermal needs of the avionics system.

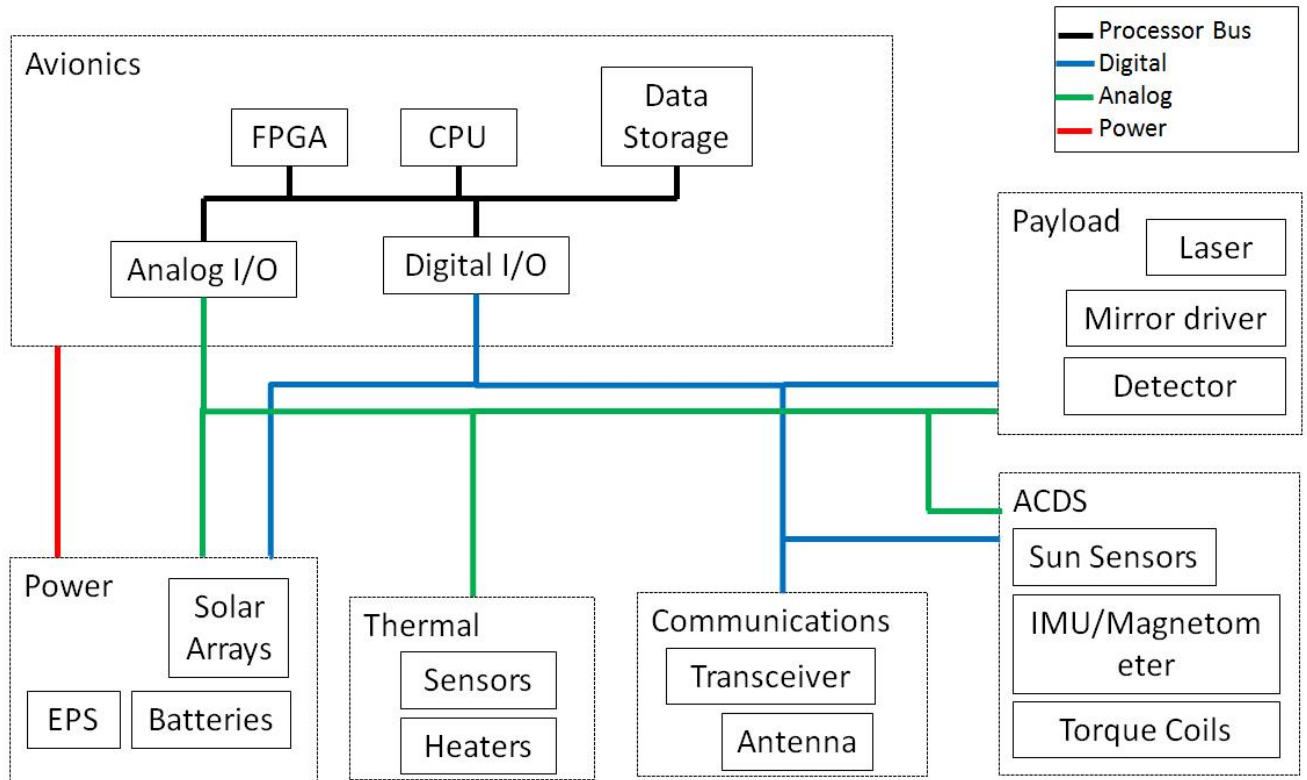| Output	Value
Power (Standby)	0.5 W
Power (Data Capture)	1.25 W
Power (Downlink/Uplink)	0.5 W
Power (Safe Mode)	0.5 W
Mass	0.062 kg
Volume	0.104 U

Figure 15: Caption goes here...

3.5.6 Risks - ZC

There are two risks that avionics faces currently. One risk which is a high consequence, but a very low likelihood is that the system will not be capable of processing all of the incoming data for payload. Payload is outputting a lot of data, and because the design of the code that will do the process has not yet been done, it is unclear how quickly Avionics will be able to process incoming data. The other risk that Avionics is currently faces, which is of very low likelihood, but very high consequence, is that it will not be capable of providing the required latency for Payload or for ADCS. Research needs to be conducted to determine how fast avionics can receive and issue orders to ensure that the computer is fast enough for the system. If it is not fast enough there could be major failures in the system because the attitude of the craft is not correct.

3.5.7 Future Work - ZC

The future work that needs to be conducted is that there should be work done to determine a new solution to interfacing with Payload. The mirror driver interfaces with USB 2.0, however the computer is not able to interface with this. So work should be done into determining how to resolve this. One other thing that should be looked into is ensuring that the system can run all of the necessary calculations at the required speed so that all of the payload data can be processed and sent to the ground. If all of the data cant be processed, it would be difficult to complete our science goals.

3.6 Attitude Determination and Control System

3.7 Thermal

3.8 Structures

4 Conclusion - AW

In this paper it has been shown that a low-cost, quick-access mission can be carried out on a 3U CubeSat platform in order to demonstrate MEMS deformable mirror technology on-orbit. Continued iterations of the system design based on the current system risks and outlined in the section on future work need to be carried out in order to optimize the design.

4.1 Risk Summary - AW

Although, at this stage in the design the DeMi demonstration system closes, the mission is still confronted with a number of risks (see Figure 16). Due to the fact that there is only a 9% margin instead of an 18% margin between the power required and the power that can be supplied to the system, there is a high consequence, medium likelihood risk (PO1) that there will not be enough power to supply the system in order to carry out the mission.

There is also a risk (S1) that the center of mass of the structure could move out of range. With the current design, the center of mass is within range. However, since at this stage in the design there still exists the possibility that masses and positions of the parts may change, the center of mass could potentially move out of range. This risk is low likelihood but high consequence.

Two risks exist regarding the avionics subsystem. The first, a low likelihood, high consequence risk (AV1), is that the avionics subsystem will not be capable of processing all of the incoming data. The second (AV2), regards the avionics system not being capable of providing the required latency for the Payload and ADCS subsystems.

Additionally, there is a low consequence, low likelihood risk (AD1) that ADCS will exceed the system mass budget. Since a trade between mass and power was made in the design of the torque coils, both the mass and power budgets of the system are tight, and the system components and design still have the potential to change in this stage of the design, if the torque coil design needs to change in order to reduce the power draw of the system, the mass might increase to above the maximum set by the CubeSat regulations. However, this is a low consequence, low likelihood risk since currently the system mass is under the maximum for a 3U CubeSat with over a 30% margin.
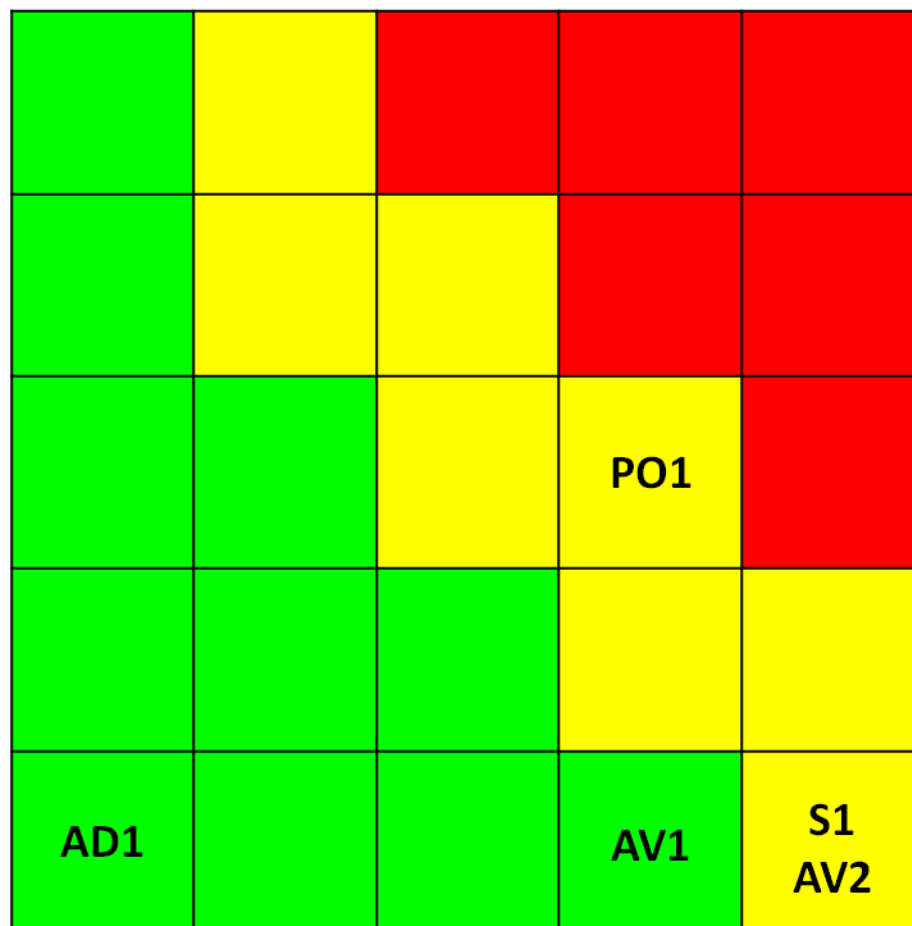

Figure 16: Systems level risk chart.

4.2   Future Work - AW

More iterations in the design process need to be carried out before the design can be completed. Future work for the DeMi demonstration includes creating more detailed models of the temperature dependence of battery and solar panel performance and the temperature gradient across the satellite in order to more accurately calculate the power that can be supplied to the system and to determine whether the proposed heating design will be effective. Additionally, as the design continues to mature, the structural model will need to continue to be updated. It also needs to be verified that the structure and components will survive the launch environment. In addition, further research needs to be conducted on the construction and use of the measuring tape antenna. More research and analysis needs to be carried out regarding the interface with payload and it must be confirmed that the avionics system can process all information at the required speed. Finally, ADCS needs to create more accurate models of external disturbances and an attitude control loop.

5   Acknowledgments

A
Requirements

Requirements go here.

B

Link Budgets

References

[1] Image from Clyde Space. URL `http://www.clyde-space.com/cubesat_shop/solar_panels_-_deployable`, (visited May 05, 2013).

[2] (2012). "CubeSat Kit – In Space." URL `http://www.cubesatkit.com/content/space.html`, (visited May 05, 2013).

[3] Strain, A, (February 14, 2011). "User Manual: CubeSat 3U Electronic Power System." URL `http://www.clyde-space.com/documents/2471`, (visited May 05, 2013).

[4] Worrall, K, (March 14, 2011). "CubeSat Power Distribution Module User Manual." URL `http://www.clyde-space.com/documents/2560`, (visited May 05, 2013).

[5] McLaren, V, (April 28 2010). "User Manual: Standalone 30Wh Battery." URL `http://www.clyde-space.com/documents/1902`, (visited May 05, 2013).

[6] (March 16 2012). "CubeSat Solar Panels." URL `http://www.clyde-space.com/documents/2625`, (visited May 05, 2013).

[7] Cahoy, K. L., A. Marinan, B. Novak, C. Kerr, M. Webber. *Wavefront control in space with MEMS deformable mirrors*, Photonics West, MEMS Adaptive Optics VII, Vol. 8617, SPIE, Washington, D.C., 2013.

[8] Demtroeder, W. *Laser Spectroscopy: Basic Concepts and Instrumentation*, 3rd ed. Berlin: Spring-Verlag, 2003.

[9] DICE (Dynamic Ionosphere CubeSat Experiment), DICE-1 and DICE-2, eoPortal, `https://directory.eoportal.org/web/eoportal/satellite-missions/d/dice`, Accessed 4/2013.

[10] Greivenkamp, John E. *Field Guide to Geometrical Optics*, Bellingham, WA: SPIE, 2004. Print.

[11] "JPL LMRST Antenna Deployment Test", `http://www.youtube.com/watch?v=DSvHKzM8scc`, Accessed 4/2013.

[12] "ITU-R P.676-9", `http://www.itu.int/dms_pubrec/itu-r/rec/p/R-REC-P.676-9-201202-I!!PDF-E.pdf`, Accessed 4/2013.

[13] Nicoletta, C. A. and A. G. Eubanks. *Effect of Simulated Space Radiation On Selected Optical Materials.* Washington, D.C.: National Aeronautics and Space Administration, 1972.

[14] Pozar, David M., *Microwave and RF Design of Wireless Systems*, Wiley, New York City, NY, 2001.

[15] Clyde Space. CubeSat Shop. [Online]. `http://www.clyde-space.com/cubesat_shop/obdh/364_mission-interface-computer-grande-em`, visited May 5, 2013.

[16] Kim. (2000). *Simulation Study of A Low-Low Satellite-to-Satellite Tracking Mission.* (Doctoral dissertation) The University of Texas at Austin, TX.

[17] Tyson, Robert K. and Benjamin W. Frazier. *Field Guide to Adaptive Optics.* Bellingham, WA: SPIE Press, 2012. Internet resource.

[18] Wertz, James, *Space Mission Engineering: The New SMAD*, Microcosm Press, Hawthorne, CA, 2011.

Figure 17: Uplink Budget

Uplink_Budget.pdf

Figure 18: Downlink Budget

Downlink_Budget.pdf